International Journal of Nanomedicine

Dovepress

open access to scientific and medical research

Open Access Full Text Article

ORIGINAL RESEARCH

Sustainable Release Selenium Laden with SiO_2 Restoring Peripheral Nerve Injury via Modulating PI3K/AKT Pathway Signaling Pathway

Jianguo Song[1,*], Huanliang Meng[2,*], Guoying Deng[1], Haodong Lin[1]

[1]Trauma Center, Shanghai General Hospital, Shanghai Jiao Tong University School of Medicine, Shanghai, 201620, People's Republic of China; [2]Department of Orthopedics, Shanghai General Hospital, Shanghai Jiao Tong University School of Medicine, Shanghai, 200080, People's Republic of China

*These authors contributed equally to this work

Correspondence: Guoying Deng; Haodong Lin, Trauma Center, Shanghai General Hospital, 650 New Songjiang Road, Shanghai, 201620, People's Republic of China, Email guoying.deng@shgh.cn; haodong.lin@hotmail.com

Background: Inhibiting ROS overproduction is considered a very effective strategy for the treatment of peripheral nerve injuries, and Se has a remarkable antioxidant effect; however, since the difference between the effective concentration of Se and the toxic dose is not large, we synthesized a nanomaterial that can release Se slowly so that it can be used more effectively.

Methods: $Se@SiO_2$ NPs were synthesized using a mixture of Cu_{2-x} Se nanocrystals, and the mechanism of action of $Se@SiO_2$ NPs was initially explored by performing sequencing, immunofluorescence staining and Western blotting of cellular experiments. The mechanism of action of $Se@SiO_2$ NPs was further determined by performing behavioral assays after animal experiments and by sampling the material for histological staining, immunofluorescence staining, and ELISA. The effects, mechanisms and biocompatibility of $Se@SiO_2$ NPs for peripheral nerve regeneration were determined.

Results: Porous $Se@SiO_2$ was successfully synthesized, had good particle properties, and could release Se slowly. CCK-8 experiments revealed that the optimal experimental doses were 100 μM H_2O_2 and 200 μg/mL $Se@SiO_2$, and RNA-seq revealed that porous $Se@SiO_2$ was associated with cell proliferation, apoptosis, and the PI3K/AKT pathway. WB showed that porous $Se@SiO_2$ could increase the expression of cell proliferation antigens (PCNA and S100) and antiapoptotic proteins (Bcl-2), decrease the expression of proapoptotic proteins (Bax), and increase the expression of antioxidative stress proteins (Nrf2, HO-1, and SOD2). EdU cell proliferation and ROS fluorescence assays showed that porous Se@SiO2 promoted cell proliferation and reduced ROS levels. The therapeutic effect of LY294002 (a PI3K/AKT pathway inhibitor) was decreased significantly and its effect was lost when it was added simultaneously with porous $Se@SiO_2$. Animal experiments revealed that the regenerated nerve fiber density, myelin thickness, axon area, gastrocnemius muscle wet-to-weight ratio, myofiber area, sciatic nerve function index (SFI), CMAP, apoptotic cell ratio, and levels of antioxidative stress proteins and anti-inflammatory factors were increased following the administration of porous $Se@SiO_2$. The levels of oxidative stress proteins and anti-inflammatory factors were significantly greater in the $Se@SiO_2$ group than in the PNI group, and the effect of LY294002 was decreased significantly and was lost when it was added simultaneously with porous $Se@SiO_2$.

Conclusion: $Se@SiO_2$ NPs are promising, economical and effective Se-releasing nanomaterials that can effectively reduce ROS production, inhibit apoptosis and promote cell proliferation after nerve injury via the PI3K/AKT pathway, ultimately accelerating nerve regeneration. These findings could be used to design new, promising drugs for the treatment of peripheral nerve injury.

Keywords: $Se@SiO_2$, PI3K/AKT, PNI, antioxidative stress, apoptosis

Introduction

The high prevalence of peripheral nerve damage can be attributed to the vulnerability of peripheral nerves to physical trauma, such as automobile accidents.[1] Compared with that of the central nervous system, the capacity of peripheral nerves to be reproduced is limited.[2,3] Natural disasters and armed conflicts can cause a substantial increase in peripheral

Received: 26 February 2024
Accepted: 23 July 2024
Published: 1 August 2024

Graphical Abstract

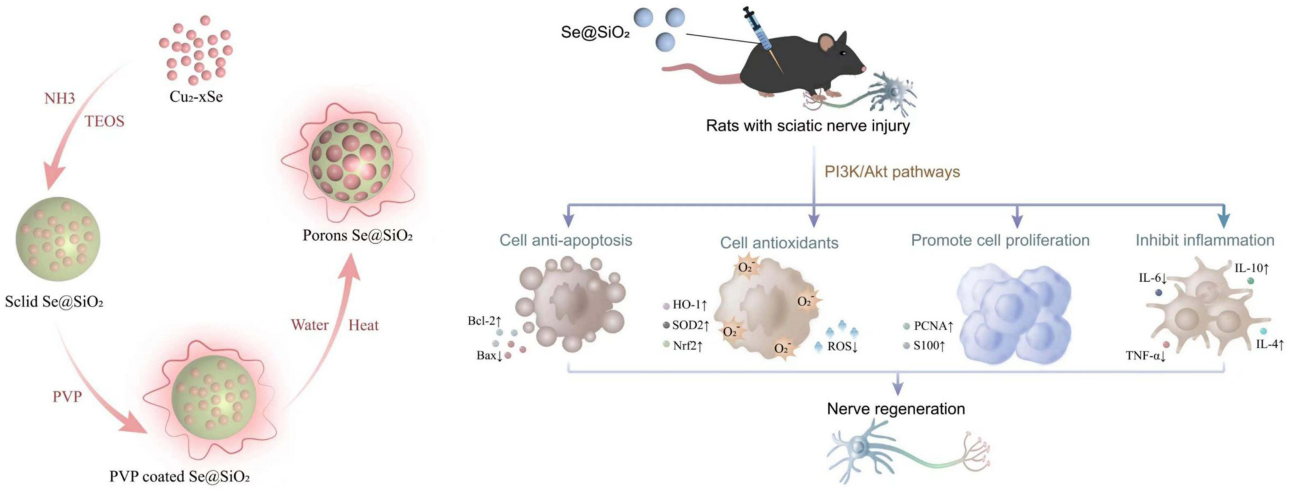

nerve injuries (PNIs) within a short period.[4] According to statistics, thousands of people worldwide suffer from diseases related to peripheral nerve injuries every year,[5] consuming a large amount of medical resources each year. Considering the limited regenerative capacity of nerve tissue, managing peripheral nerve damage poses challenges.[6,7] For instance, the complex nature of peripheral nerves and the formation of fibrous scar tissue can impede the nerve repair process.[8]

After peripheral nerve injury, the distal end of the nerve undergoes Wallerian degeneration,[9] ie, total destruction of myelin sheaths, after which the Schwann cells(SCs) reactivate the expression of pro-neural regeneration genes through a process of dedifferentiation.[10] Dedifferentiated SCs can secrete neurotrophic and inflammatory factors to attract inflammatory cells, such as macrophages, to the site of injury to phagocytose myelin debris,[11] which helps to promote the extension of axons to end organs and create a beneficial microenvironment for nerve regeneration. However, excessive macrophage aggregation often leads to excessive formation of local reactive oxygen species (ROS),[12] and the overproduction of ROS disrupts the balance between oxidation and antioxidants, leading to impaired mitochondrial function and dynamics,[13] apoptosis, and endoplasmic reticulum stress. Therefore, the inhibition of excessive ROS production is a key component in promoting nerve regeneration.

Nuclear factor erythroid 2-related factor 2 (Nrf2) is an important transcription factor.[14] Nrf2 is recognized as a biomarker of neuronal stress and plays an important role in exogenously induced neuronal stress responses.[15] Heme oxygenase 1 (HO-1) is an enzyme that catalyzes the rate-limiting step in the oxidative degradation of heme to ferrous ions, CO, and bilirubin,[16] and also serves as a key Nrf2-dependent transcription factor mediating antioxidant or anti-inflammatory responses.[17] The PI3K/AKT pathway is involved in the activation of the Nrf2/HO-1 signaling pathway, and is closely related to cell growth and development.[18] Neural stem cells (NSCs) are a class of parent cells with differentiation potential and self-renewal ability that can give rise to neurons, oligodendrocytes, and other cell types through unequal division.[19] During nerve injury, the PI3K/AKT signaling pathway is activated to positively induce the differentiation of NSCs to neurons and shorten the cellular interphase to enable them to rapidly enter the cytokinesis phase,[20] and the expression of proliferation markers such as PCNA and S100 is also significantly increased,[21] thus accelerating the proliferation and differentiation of unmyelinated and myelinated SCs. The expression of proliferation markers such as PCNA and S100 also increases significantly, thus accelerating the proliferation and differentiation of neuronal cells, promoting the encapsulation of axons by unmyelinated and myelinated SCs and increasing the synthesis of myelin proteins in myelinated SCs, which ultimately promotes the formation of myelin sheaths.[22] Therefore, the search for a drug that promotes the activation of the PI3K/AKT signaling pathway seems extremely relevant.

Selenium (Se), a vital micronutrient in the human body,[23] plays an indispensable role in the functions of two major antioxidant kinases: glutathione peroxidase (GPx) and thioredoxin reductase.[24] Its absence has been associated with cancer development, viral infections, and various cardiovascular conditions, such as Keshan disease.[25] Studies suggest that consuming 200 mg of Se daily can significantly decrease the risk of cancer.[26] Se plays a role in preventing ischemia–reperfusion injury by eliminating ROS and safeguarding liver cells from oxidation.[27] Moreover, research has shown that Se can regulate iron-induced cell death through the activation of the Hippo pathway, providing enhanced protection for brain neurons.[28] Se can also inhibit intestinal iron-induced death by activating the PI3K/AKT signaling pathway, thereby protecting the intestinal tract from inflammatory damage;[29] another study has shown that selenium promotes endometrial repair by activating the PI3K/AKT signaling pathway in vitro, which promotes cell proliferation and migration.[30] Therefore, selenium, an effective antioxidant that activates the PI3K/AKT pathway, has promising applications in disease management.

Silica nanoparticles (NPs) have been extensively investigated due to their unparalleled advantages, such as excellent compatibility, an adaptable pore structure, cost-effective production feasibility, and manageable therapeutic effects.[31] In a recent study by Liu et al, porous Se@SiO_2 nanocomposites were introduced as an innovative strategy for the controlled release of Se NPs.[32] These NPs exhibited exceptional biocompatibility in healthy cells and served as efficient drug carriers. Porous Se@SiO_2 nanocomposites not only minimize the risks associated with selenotoxicity but also demonstrate remarkable bioactivity both in laboratory settings and in living organisms.[33] Recent studies have revealed that porous Se@SiO_2 NPs possess advantageous antioxidant properties and safety characteristics by promoting muscle regeneration through the regulation of mitochondrial oxidation processes.[34] However, documented evidence on how these particles influence the restoration of functionality within the perinucleolar compartment or relevant molecular mechanisms is currently unavailable.

This study investigated the potential neuroprotective effects of Se@SiO_2NPs on axon regeneration and functional restoration following PNI, with the aim of exploring the underlying molecular mechanisms involved. These findings revealed that Se@SiO_2 NP therapy effectively reduced SC apoptosis, decreased ROS levels, promoted myelin regeneration, and facilitated functional recovery after PNI. Moreover, based on our findings from both in vitro and in vivo experiments, these beneficial effects are likely mediated by activating the PI3K/AKT pathway and inhibiting oxidative stress. Our study indicated that Se@SiO_2 NPs can be used to treat PNI effectively and are good candidates for clinical trials.

Materials and Methods

Reagents and Antibodies

H_2O_2 (10%) was purchased from Sigma, and ROS (S0033S), EdU cell proliferation kit (C0071S), and MDA (S0131S), GSH (S0053), SOD (S0101S), CAT (S0051), TNF-α (PT516), IL-4 (PI615), IL-6 (PI328), and IL-10 (PI525) assay kits were purchased from Beyotime. Antibodies against p-Akt (ab8805), Bax (ab32503), Bcl-2 (ab182858), GAPDH (ab9485), HO-1 (ab305290), SOD2 (ab68155), PCNA (ab92552), S100 (ab52642), Nrf2 (ab62352), and Akt (ab179463), and the PI3K/AKT inhibitor LY294002 (ab146593) were purchased from Abcam.

Preparation and Characterization of Porous Se@SiO_2 NPs

Porous Se@SiO_2 NPs were compounded using the methodology employed in the authors' prior study.[32] The nitrogen-synthesized Cu_{2-x} Se nanocrystal mixture was meticulously blended with 20 mL of n-hexane, 20 mL of n-hexanol, 2 mL of Triton X-100, 0.6 mL of deionized water, and 0.08 mL of ethyl orthosilicate. Additionally, 0.1 mL of ammonia was added. With the breakdown of orthosilicate, silica was enclosed in Se quantum dots, which were oxidized to create solid Se@SiO_2 NP nanospheres. The polyvinylpyrrolidone solution was added to 10 mg/mL of the substance, and the resulting porous structures were created by etching in hot water. Transmission electron microscopy (TEM) (HT7700, HITACHI, Tokyo, Japan) and a D/max2550 X-ray diffractometer (Cu K-α radiation; Rigaku, Tokyo, Japan) were utilized to analyze the porous Se@SiO_2 NPs.

Animals

We obtained 20 male Sprague–Dawley (SD) rats weighing between 220 and 240 grams from the Laboratory Animal Center of Shanghai General Hospital in Shanghai, China. The Animal Experimental Ethics Committee of Shanghai General Hospital approved the use of animals in this study under approval number 2022AW022. Animals in laboratories received care and were used according to the National Institutes of Health (NIH) guidelines.

PNI Model and Drug Injection

The generation of the animal model involved a straightforward process. Anesthesia was administered to the animal, and a skin incision was created to expose the right sciatic nerves. Subsequently, those nerves were crushed using one vascular clip, which securely held the sciatic nerve 6 mm proximal to the sciatic incision from both ends, with a force of 30 g applied for 1.5 minutes. The incised skin was then sutured. Postoperatively, the animals were stochastically assigned to 4 groups (n = 5 rats per group): the sham surgery, PNI, Se@SiO_2 NP, and Se@SiO_2 NP + LY294002 groups. The sham group underwent the same surgical procedure but without PNI. Rats in the Se@SiO_2 NP group received an intraperitoneal injection of a Se@SiO_2 NP solution (9 mg/kg), and those in the Se@SiO_2 NP + LY294002 group received an intravenous injection of LY294002 (a PI3K inhibitor, 0.3 mg/kg/day[35]) following the injection of the Se@SiO_2 NP solution.[22] In addition to the rats in the sham operation group, the rats in the PNI group were treated with the same volume of saline solution. After twenty-eight days, all the rats were subjected to a walking pattern analysis and electrophysiological assessments and subsequently euthanized.

Walking Pattern Analysis

The walking pattern of the rats was examined in a passageway measuring 100×10 x 15 cm, with the base wrapped in white paper. The back of each rat was marked with black ink. Bain et al utilized colored footprints to calculate the sciatic nerve function index (SFI) with the following formula: SFI = −38.3 × (EPL - NPL)/NPL + 109.5 × (ETS - NTS)/NTS + 13.3 × (EIT - NIT)/NIT - 8.8.[23] In this equation, E is the right hind limb, N is the left hind limb, PL is the distance between the heel and the front toe, and TS refers to the distance between the 1st toe and the 5th toe. In addition, the IT refers to the distance between the 2nd toe and the 4th toe. For the SFI, 0 indicates normal impairment, and −100 indicates complete impairment. After surgery, three observers performed testing until day 21.

Electrophysiological Assessments

Under anesthesia, the surgical site was reopened at twenty-eight days after surgery to reveal the sciatic nerve. In the gastrocnemius, complex muscle action potentials (CMAPs) and latency were measured after electrical stimulation (2 mV) was applied to the proximal sciatic nerve.

HE Staining, LFB Staining, TUNEL Staining and Myelin Analysis

Twenty-eight days after surgery, 5 mm of sciatic nerve tissue from each group was removed from the right side of the injury center, stored in a freezer at −80°C, placed in 4% paraformaldehyde for fixation, trimmed, dehydrated, and embedded in paraffin wax after 24 h. After deparaffinization, the sections were stained with a hematoxylin solution to stain the nuclei of the cells, stained with eosin for cytoplasmic staining, dehydrated and sealed. For LFB staining, the slices were incubated in an LFB staining solution and then placed in 70% ethanol and 0.05% lithium carbonate solution for differentiation, and then restained with eosin to seal the slices. For TUNEL staining, the slices were incubated in a TUNEL reaction mixture, rinsed with PBS, converter-POD was added to the slices, the sections were rinsed with PBS, DAB substrate was added, the sections were restained with hematoxylin, and the sections were then sealed after dehydration. The above stained slices were placed under a fluorescence microscope for observation. For the myelin analysis, the sciatic nerve was removed and placed in 2.5% glutaraldehyde buffer overnight. Then, the sample was fixed with a 1% osmium solution, rinsed with PBS, dehydrated with a gradient of ethanol concentrations, embedded, trimmed to a trapezoidal shape, and sectioned. The slices were 80 mm thick, and after staining with a lead citrate

solution and a saturated solution of 50% hydrogen peroxide acetate in ethanol, slices were observed under a transmission electron microscope. Image-Pro Plus software was used for myelin data analysis.

Evaluation of the Gastrocnemius Muscle

Twenty-eight days after surgery, we carefully weighed and photographed the gastrocnemius muscles of both the control and experimental rats. The weight recovery rate of the gastrocnemius muscle was determined with the formula Wr(%)=[Ws/Wn]×100. Paraffin sections (6 μm thick) were prepared from the gastrocnemius muscle, followed by Masson's trichrome staining, with three different views obtained for each section. Using Image-Pro Plus software, the cross-sectional regions of muscle fibers (a) and collagen fibers (b) were calculated. The proportion of the collagen fiber region was determined using the formula c(%)=[b/(a+b)]×100, where (a) represents the cross-sectional area of muscle fibers, (b) denotes the cross-sectional area of collagen fibers, and (c) signifies the percentage.

Measurement of MDA, GSH, SOD, CAT, TNF-α, IL-4, IL-6, and IL-10 Levels

Twenty-eight days after surgery, 5 mm of the sciatic nerve centered on the right side of the injury was removed, and the nerve was stored at −80°C. Subsequently, malondialdehyde (MDA) levels were measured to assess lipid peroxidation, ie, 0.2 mL of MDA assay solution was added to 0.1 mL of previously prepared standards and samples, heated at 100°C for 15 min, cooled in a water bath to room temperature, and centrifuged at 1000 × g for 10 min at room temperature. Afterward, the absorbance was measured at 532 nm using an spectrophotometer. The glutathione (GSH) level in the cells was measured using a glutathione assay kit, ie, 100 μL of sample and standard were prepared, and then 150 μL of GSH assay solution was added and incubated for 5 min at room temperature. Subsequently, the absorbance was measured at 412 nm using an spectrophotometer. SOD activity was determined by performing a xanthine oxidase assay, ie, 160 μL of WST-8 assay solution and 20 μL of starter working solution were added to 20 μL of previously prepared standards and samples, and the absorbance was measured at 450 nm. CAT activity was studied by performing a catalase (CAT) activity assay, ie, 4 μL and 20 μL of each of the samples were prepared with different concentrations of hydrogen peroxide solution, and 200 μL of the color development working solution was added simultaneously. The absorbance was measured at 520 nm after an incubation at 25°C for 15 min. Tumor necrosis factor α (TNF-α), interleukin 4 (IL-4), interleukin 6 (IL-6) and interleukin 10 (IL-10) levels were detected by adding the samples and different concentrations of standards to the wells at 100 μL/well, washing the plate 5 times, adding 100 μL of biotinylated antibody to each well and incubating the plate for 60 min at room temperature. After the plates were washed 5 times, 100 μL of horseradish peroxidase was added to each well, 100 μL of color developer TMB solution was added to each well, the plates were incubated at room temperature in the dark for 15–20 minutes, and finally, 50 μL/well termination solution was added. The absorbance at 450 nm was measured immediately after mixing.

Evaluation of in vivo Safety

The hearts, livers, spleens, lungs and kidneys of the rats from each group were collected at twenty-eight days after surgery, and HE staining was performed in the same manner as described above to observe the presence of edema, congestion and necrosis.

RSC96 Culture and Cell Viability Assay

The RSC96 SC system was provided by the ScienCell Research Laboratory. We seeded the cells in 96-well plates (10^4 cells/well) and incubated them with various concentrations of H_2O_2 for twelve hours. Then, CCK-8 solution (Beyotime, China) was added to each well, and the plates were subsequently incubated at 37°C for another two hours. The optical density was measured 450 nm using an spectrophotometer from Thermo Fisher Scientific. After the cells were seeded into 96-well plates (10^4 cells/well), they were treated with different concentrations of $Se@SiO_2$ (0, 50, 100, 200, 300, and 400 μg/mL) for two hours. The appropriate concentration of H_2O_2 for treatment was determined to be 100 μM. In subsequent experiments, following the addition of 100 μM H_2O_2, 10 μL of CCK-8 solution was added to each well. In addition, the cells were incubated for two more hours at 37°C. The optical density was determined at 450 nm using an

spectrophotometer from Thermo Fisher Scientific. Every experiment was conducted no less than three times. Prior to the introduction of Se@SiO_2 NPs, the cells were pretreated with LY294002 (20 μm), a PI3K inhibitor, for two hours to investigate the effect of PI3K/AKT activation on oxidative damage more comprehensively.

Intracellular ROS Production and Cell Proliferation Assays

A ROS assay kit (DCFH-DA, S0033, Beyotime, China) was used to measure intracellular ROS production, and a proliferation assay kit (C0071S, Beyotime, China) was used to analyze cellular proliferation. SCs were cultivated in a 12-well plate at a density of 5×10^4 cells/mL and incubated for 36 h. The cells were divided into four groups and incubated with the appropriate reagents. Subsequently, the cell fluorescence in three random regions in each group was photographed with a two-photon confocal fluorescence microscope (Zeiss, China). ImageJ software was used for the quantitative analysis.

Western Blotting

We measured protein concentrations with a BCA protein assay kit. Proteins were separated on 10% SDS–PAGE gels and subsequently transferred to poly(vinylidene fluoride) (PVDF) membranes. After an incubation with 4% nonfat milk for 1.5 hours, the membranes were incubated overnight at 4°C with primary antibodies. Then, the membranes were incubated with secondary antibodies for 1 h and rinsed 3 times with TBST. An Odyssey imaging system (Tanon) was used to detect fluorescence signals.

Statistical Analysis

The data are presented as the mean values and mean standard errors. One-way ANOVA was implemented using GraphPad Prism (software version 9.5, USA) to assess statistical significance. $p<0.05$ indicated statistical significance.

Results

Characterization of Se@SiO_2 NPs

We employed XRD analysis to identify the Se@SiO_2 NP constituents. The results revealed that the Se@SiO_2 NPs retained a crystalline structure identical to that in the native Se phase. Furthermore, the 2θ angle of the Se@SiO2 NPs shifted by approximately 23° due to the silica coating (Figure 1C). The TEM findings confirmed the successful synthesis of Se@SiO_2 NPs, which exhibited a consistent spherical morphology. The Se@SiO_2 NPs had a diameter of approximately 55 nm, and numerous minute particles were spread around the surface or within the core (Figure 1A and B). Se@SiO_2 NPs with pores were fabricated via heat treatment at 95°C, resulting in the development of a porous structure (Figure 1D). We successfully synthesized porous Se@SiO2 NPs according to previous experimental steps (Figure 1E).

Se@SiO_2 NPs Activation of the PI3K/AKT Pathway Inhibits H_2O_2-Induced Apoptosis in vitro

Activation of the PI3K/AKT pathway is closely linked to nerve axon regeneration.[36,37] We first conducted in vitro experiments to investigate the possible mechanism of Se@SiO_2 in nerve regeneration. CCK-8 assays were employed to assess the impacts of varying concentrations of H_2O_2 on SC activity. H_2O_2 effectively reduced cell viability up to a maximum of 100 μM (Figure 2A). Consequently, 100 μM H_2O_2 was used in subsequent experiments to simulate oxidative stress-induced damage in vitro. SCs were treated with 100 μM H_2O_2 and different concentrations of Se@SiO_2 for 24 h and subsequently evaluated using the CCK-8 assay. Our results showed that maximal cell viability was achieved at a concentration of 200 μg/mL Se@SiO_2 (Figure 2B). Therefore, this concentration was selected for further in vitro experiments. We then analyzed the mechanism of action of Se@SiO_2 in nerve regeneration by performing RNA-seq. GO enrichment analysis (Figure 2C) of the H_2O_2+Se@SiO_2 group revealed that pathways associated with oxidative stress were significantly upregulated, KO enrichment analysis (Figure 2D) revealed that pathways associated with apoptosis were significantly enriched, and GSEA (Figure 2E) revealed that the PI3K/AKT pathway, which was upregulated according to the KEGG analysis, was significantly enriched in the H_2O_2+Se@SiO_2 group. We used Western blotting to analyze the levels of phosphorylated Akt, Bax, and Bcl-2

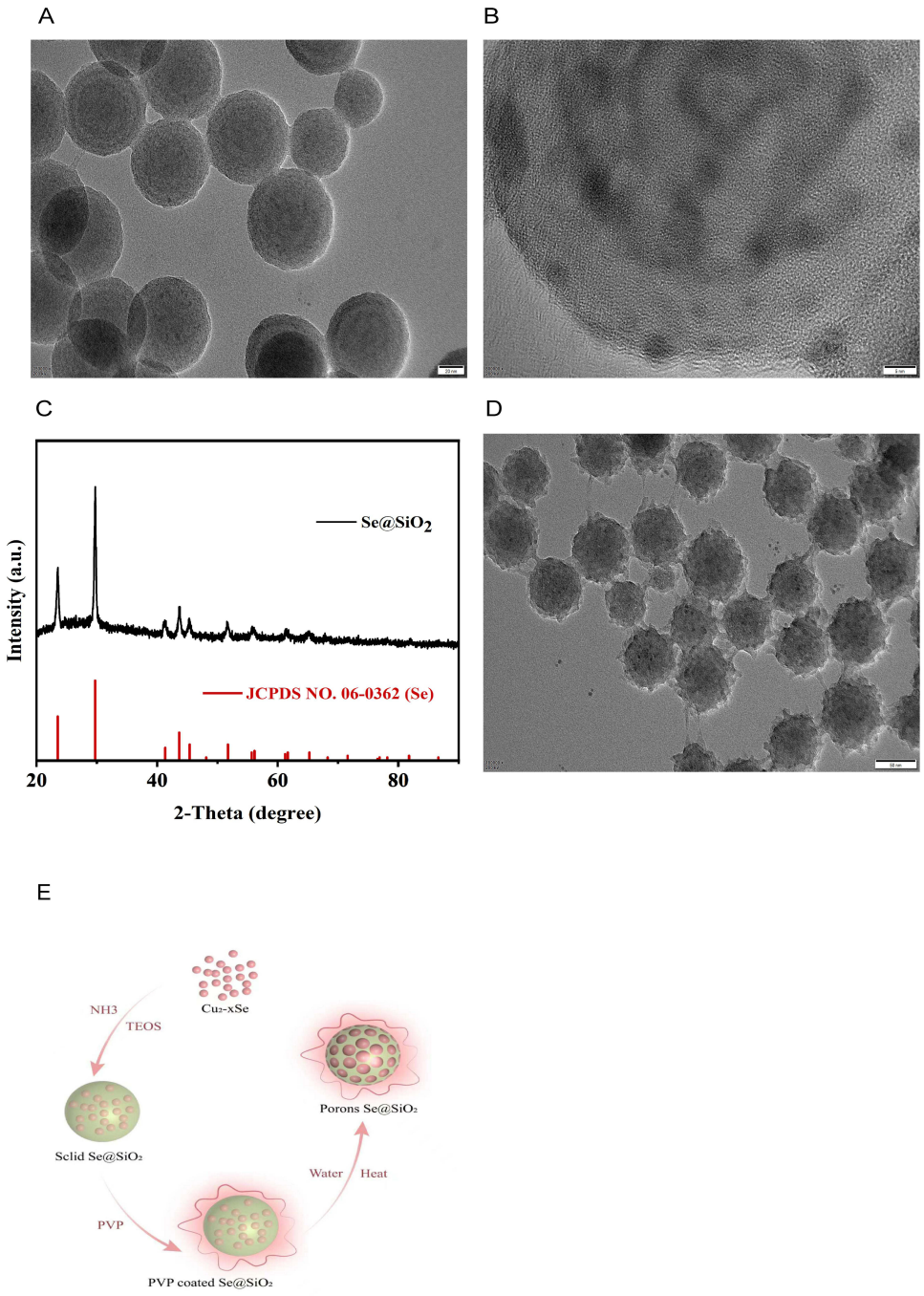

Figure 1 Examination of $Se@SiO_2$ NPs. Images of $Se@SiO_2$ nanoparticles at various magnifications: (**A**) low and (**B**) high magnifications. (**C**) The X-ray diffraction (XRD) patterns of the $Se@SiO_2$ NPs were compared to those of the standard Se hexagonal phase (JCPDS card number: 65–1876). (**D**) Medium-magnification images of porous Se@SiO2 nanocomposites. (**E**) Schematic of the method used to synthesize the Se@SiO2 NPs. TEM micrographs revealed that the $Se@SiO_2$ NPs were composed of a porous silica shell and encapsulated selenium (Se).

(Figure 2F). Bax (a proapoptotic protein) expression was far lower in the $Se@SiO_2$ group than in the H_2O_2 group (Figure 2G). The p-Akt/Akt ratio is shown in Figure 2I. Bcl-2 (an antiapoptotic protein) expression (Figure 2H) was significantly increased in the $Se@SiO_2$ group. Notably, the expression levels of Bax were higher in the $Se@SiO_2$ and LY294002 (cotreatment) groups than in the $Se@SiO_2$ treatment group, and the p-Akt/Akt ratio and the expression level of Bcl-2 were lower in the $Se@SiO_2$ and LY294002 groups than in the $Se@SiO_2$ group. Collectively, these findings suggest that $Se@SiO_2$ NPs may inhibit hydrogen peroxide-induced apoptosis through activation of the PI3K/AKT pathway.

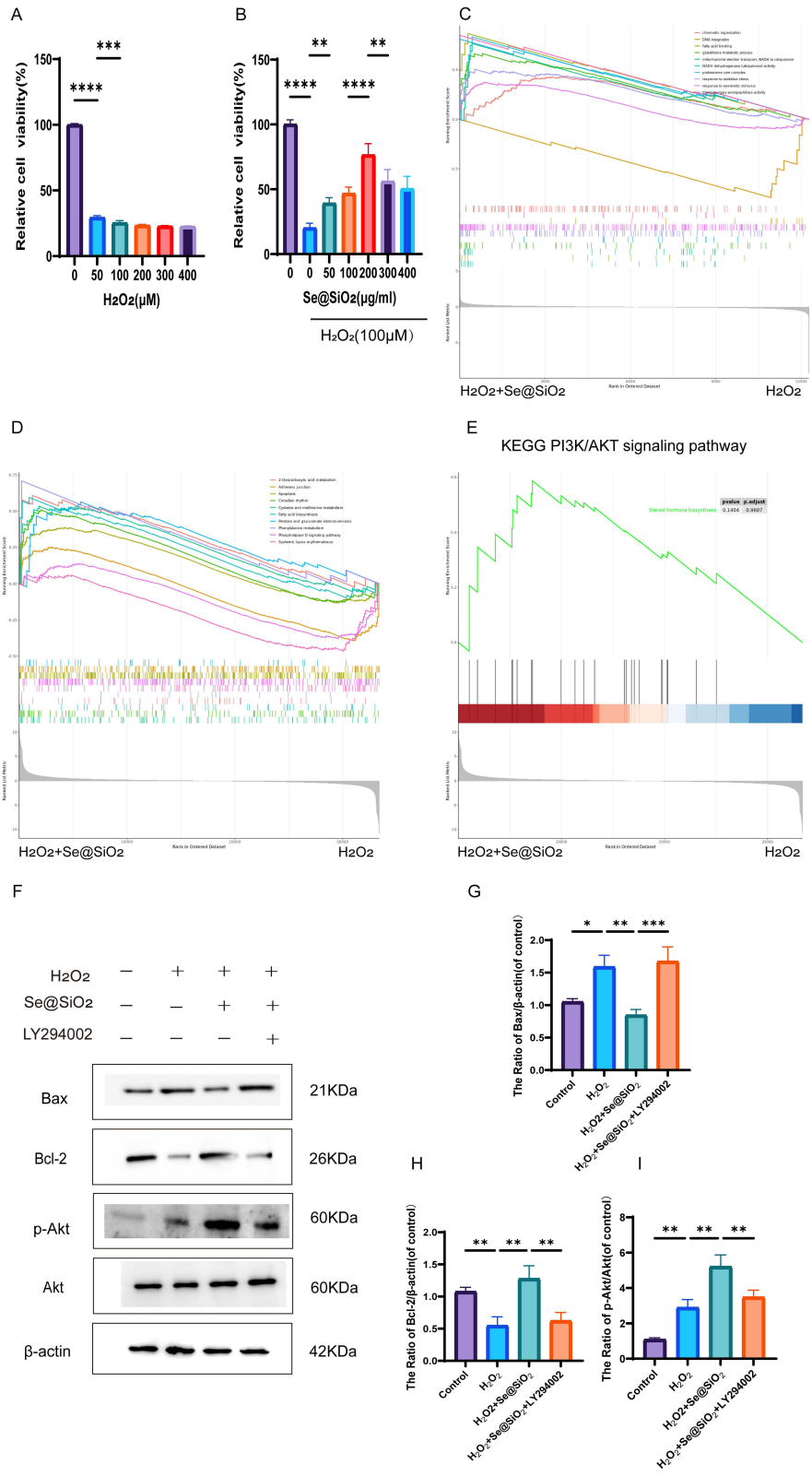

Figure 2 In vitro, Se@SiO_2 suppressed H_2O_2-triggered cell death. (**A**) The impacts of varying H_2O_2 concentrations on cell viability were evaluated using the CCK-8 assay. (**B**) The CCK-8 assay was performed to assess the viability of cells treated with various Se@SiO_2 NPs and 100 μM H_2O_2. (**C**) GO enrichment analysis of the top 10 pathways. (**D**) KEGG enrichment analysis of the top 10 pathways. (**E**) GSEA showing that enriched PI3K/AKT pathway was significantly upregulated in the Se@SiO_2 group. (**F**) Western blotting was used to assess the p-Akt, Akt, Bax and Bcl-2 protein levels. A gel imaging system was used to quantitatively evaluate p-Akt/Akt (**I**), Bax (**G**) and Bcl-2 (**H**) expression. N = 3. *P < 0.05, **P < 0.01, ***P < 0.001, and ****P < 0.0001.

$Se@SiO_2$ NPs Alleviates Oxidative Damage and Promotes Cell Proliferation Through the PI3K/AKT Pathway in vitro

Nrf2, HO-1 and SOD2 (antioxidant proteins) levels were determined via Western blotting (Figure 3A), and H_2O_2 treatment resulted in slight increases in the expression levels of these proteins. Additionally, $Se@SiO_2$ treatment promoted a substantial increase in the expression levels of these antioxidant proteins. These effects were reversed by LY294002 treatment (Figure 3D–F). The variation in ROS levels across each group was used to analyze oxidative stress. Compared to the level in the H_2O_2 treatment group, the fluorescence intensity was lower in the $Se@SiO_2$ group but much higher in the $Se@SiO_2$ + LY294002 group (Figure 3G). The fluctuations in the intracellular ROS levels were directly proportional to the fluorescence intensity (Figure 3I). These findings suggest that $Se@SiO_2$ NPs may reduce oxidative damage by activating the PI3K/AKT pathway.

Then, we examined whether $Se@SiO_2$ enhanced cell proliferation via an EdU incorporation assay. Compared with H_2O_2, $Se@SiO_2$ obviously increased the percentage of EdU-positive cells (Figure 3H–J). Nonetheless, the ratio of EdU-positive cells was notably lower in the $Se@SiO_2$ + LY294002 group. S100 is an SC marker that regulates cell proliferation, and PCNA is also a proliferation marker. We employed Western blotting to assess the levels of both proteins. The S100 and PCNA expression levels were much higher in the $Se@SiO_2$ group than in the H_2O_2 group, but the LY294002 treatment reversed this effect (Figure 3A). The quantitative analysis corroborated this trend (Figure 3B and C). These findings suggest that $Se@SiO_2$ NPs enhances cellular proliferation in vitro via the PI3K/AKT pathway.

$Se@SiO_2$ NPs Activates the PI3K/AKT Pathway in vivo to Promote Nerve Regeneration

According to the results of our preliminary in vitro experiments, $Se@SiO_2$ strongly activated the PI3K/AKT pathway. Subsequently, animal experiments were performed in which LY294002 (a PI3K/AKT inhibitor) and $Se@SiO_2$ were administered to the animal groups to examine whether the in vivo effect of $Se@SiO_2$ was similarly associated with the activation of the PI3K/AKT pathway (Figure 4F). A cross-section of the regenerated nerve was taken twenty-eight days after surgery for HE and LFB staining (Figure 4A). As measured by the density of regenerated myelin nerve fibers, the densities in the sham operation, PNI, $Se@SiO_2$, and $Se@SiO_2$ + LY294002 groups were 18359.6, 11,272.2, 16,195.1, and 13623.1/mm^2, respectively (Figure 4B). As illustrated by TEM (Figure 4A), histomorphologic parameters of reproductive nerves, such as the axon diameter, myelin thickness, and the myelinated axon region (Figure 4C–E), were analyzed. As depicted in Figure 4A–C, the average diameters of axons in the sham operation group, PNI group, $Se@SiO_2$ group, and $Se@SiO_2$ + LY294002 group were 6.80, 3.19, 6.21, and 4.25 μm, respectively; the trends for the myelin thickness and myelinated axon area were analogous. The density of axonal fibers was lower and disorganized in the PNI group, and the density of nerve fibers was greater and more ordered in the $Se@SiO_2$-treated group, with a degree of regeneration comparable to that of normal nerves. However, nerve fiber regeneration was obviously impaired after cotreatment with LY294002 and $Se@SiO_2$.

$Se@SiO_2$ NPs Activates the PI3K/AKT Pathway in vivo to Promote Recovery of Motor Function

CMAPs were recorded from each surgical side to assess whether the injection of $Se@SiO_2$ enhanced the recovery of motor conduction velocity, and the results are presented in Figure 5A. Moreover, the CMAP peak amplitude, CMAP conduction velocity, and latency were measured after biosignal acquisition and analyzed at twenty-eight days postsurgery (Figure 5B–D). CMAP signals were investigated in all the groups; nevertheless, the signal waveforms differed, suggesting varying degrees of nerve conduction recovery. As depicted in Figure 5B, the mean amplitudes of CMAPs in the sham operation group, PNI group, $Se@SiO_2$ group, and $Se@SiO_2$ + LY294002 group were 21.57, 6.67, 20.87, and 12.07 mV, respectively. These findings suggest that $Se@SiO_2$ enhances motor conduction velocity recovery and that LY294002 partially attenuates this effect. A walking pattern analysis was conducted at twenty days postsurgery. Figure 5E and F shows the results of the walking pattern analysis. The average sciatic nerve function index in the $Se@SiO_2$ group was higher than that in the PNI group and the $Se@SiO_2$ + LY294002 group, approaching that of the sham operation group. These results indicate that $Se@SiO_2$ NPs promotes motor function recovery and that LY294002 partially inhibits this effect.

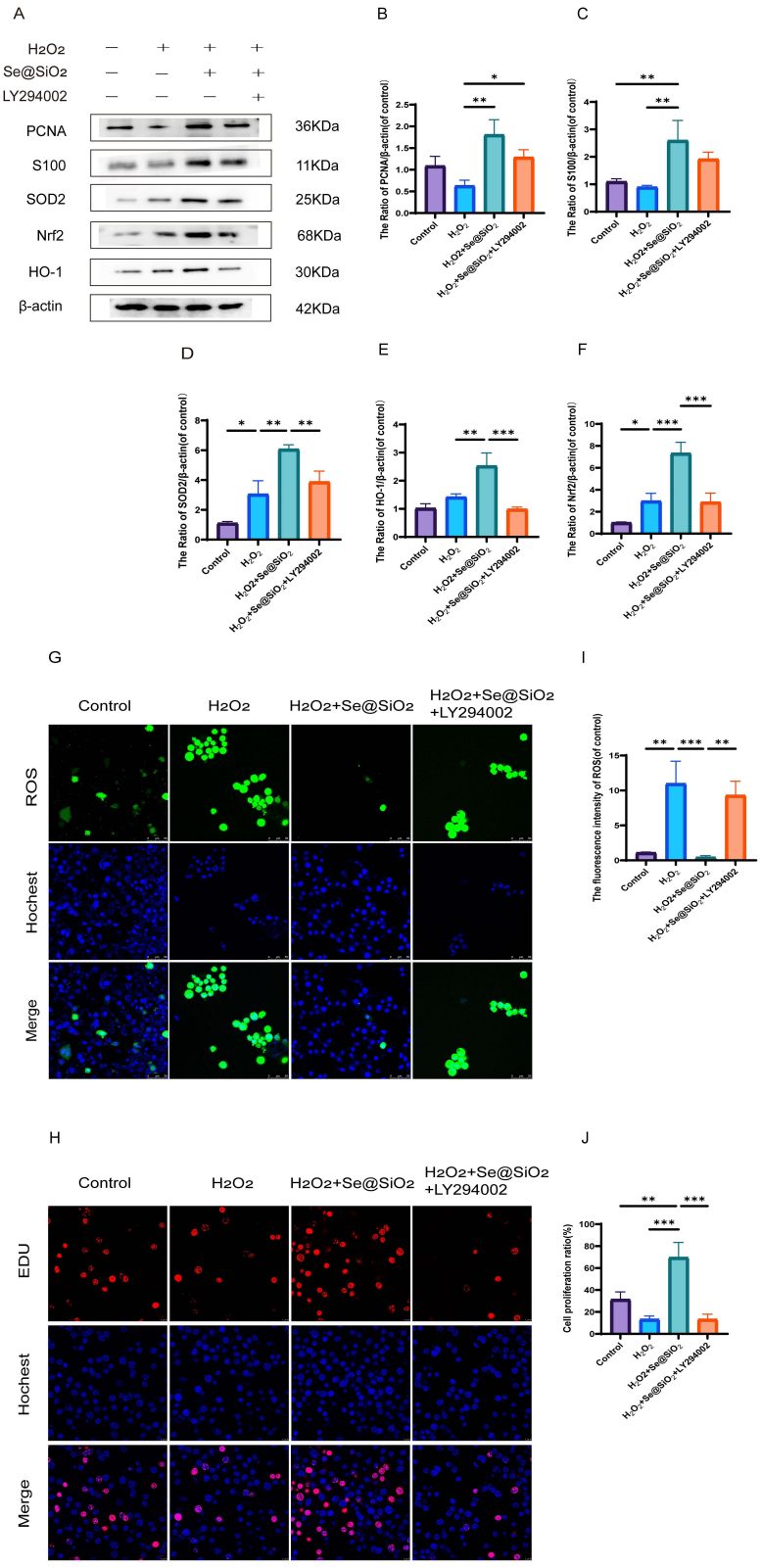

Figure 3 In vitro, Se@SiO_2 stimulates the PI3K/AKT pathway to reduce oxidative damage and increase cell growth. (**A**) Western blotting was used to assess the expression of PCNA, S100, Nrf2, SOD2, and HO-1 in Schwann cells (SCs). A gel imaging method was used to evaluate the expression of PCNA (**B**), S100 (**C**), SOD2 (**D**), HO-1 (**E**), and Nrf2 (**F**). (**G**) Reactive oxygen species (ROS) in SCs were detected by performing immunofluorescence staining with dichlorodihydrofluorescein diacetate (DCFH-DA). (**H**) Images of EdU-labeled cells from each group. (**I**) Statistical analyses were conducted to assess the fluorescence intensity of ROS. (**J**) The cell proliferation ratio in each group. N = 3. *P < 0.05, **P < 0.01, and ***P < 0.001.

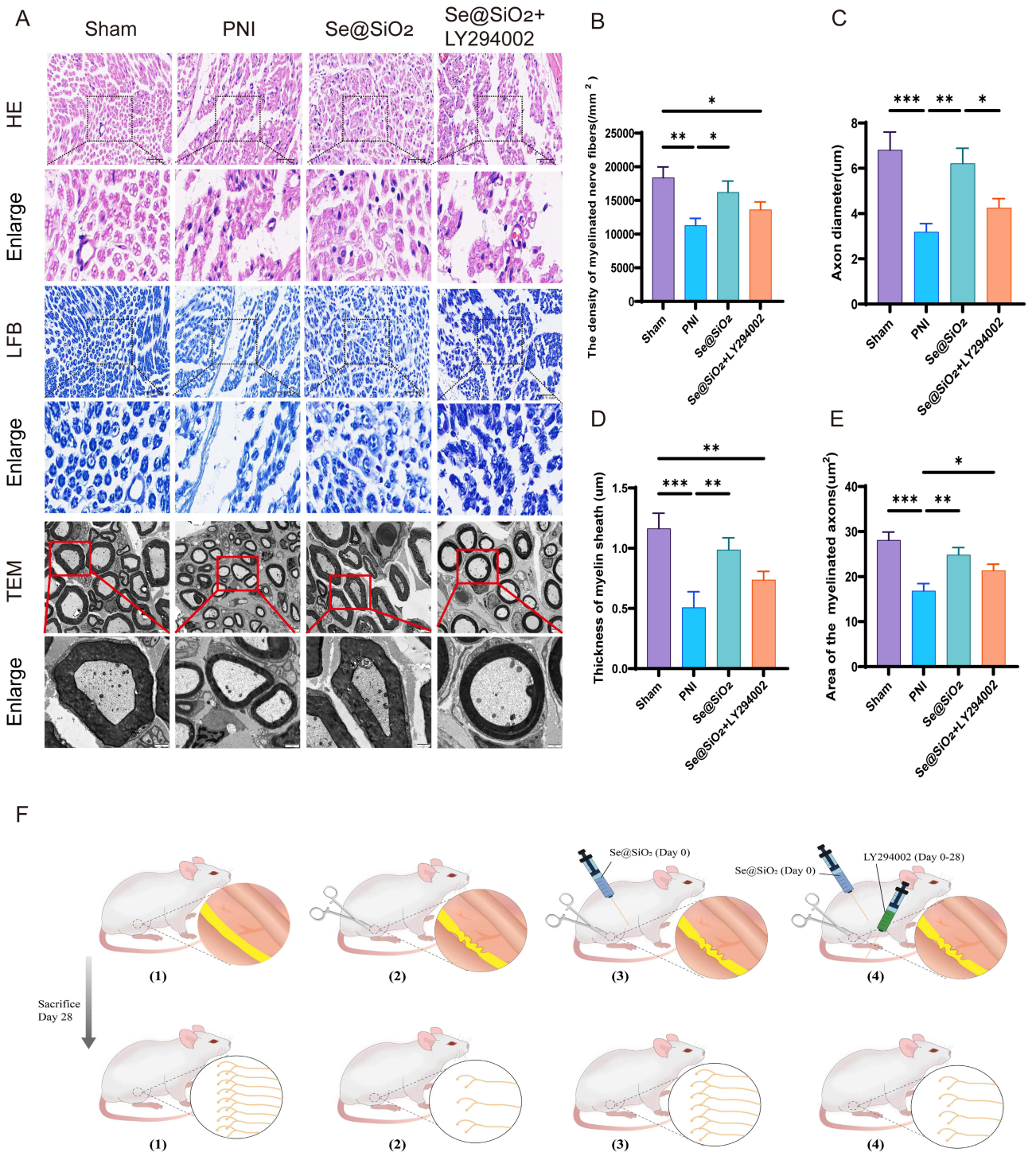

Figure 4 Histology confirmed that the Se@SiO_2 NPs stimulated axon regeneration. (**A**) We performed HE staining, Luxol fast blue (LFB) staining, and transmission electron microscopy (TEM) on cross-sections of regenerated nerves from both groups twenty-eight days after surgery. (**B**) Statistical analysis of the density of myelinated nerve fibers in the reproductive nerves of each group, including the (**C**) axon diameter, (**D**) myelin thickness, and (**E**) myelinated axon region of the regenerating nerves. (**F**) Schematic representation of animal experiments performed on the groups and tests of the effects on nerve regeneration. N = 3. *P < 0.05, **P < 0.01, and ***P < 0.001.

https://doi.org/10.2147/IJN.S460397 DovePress

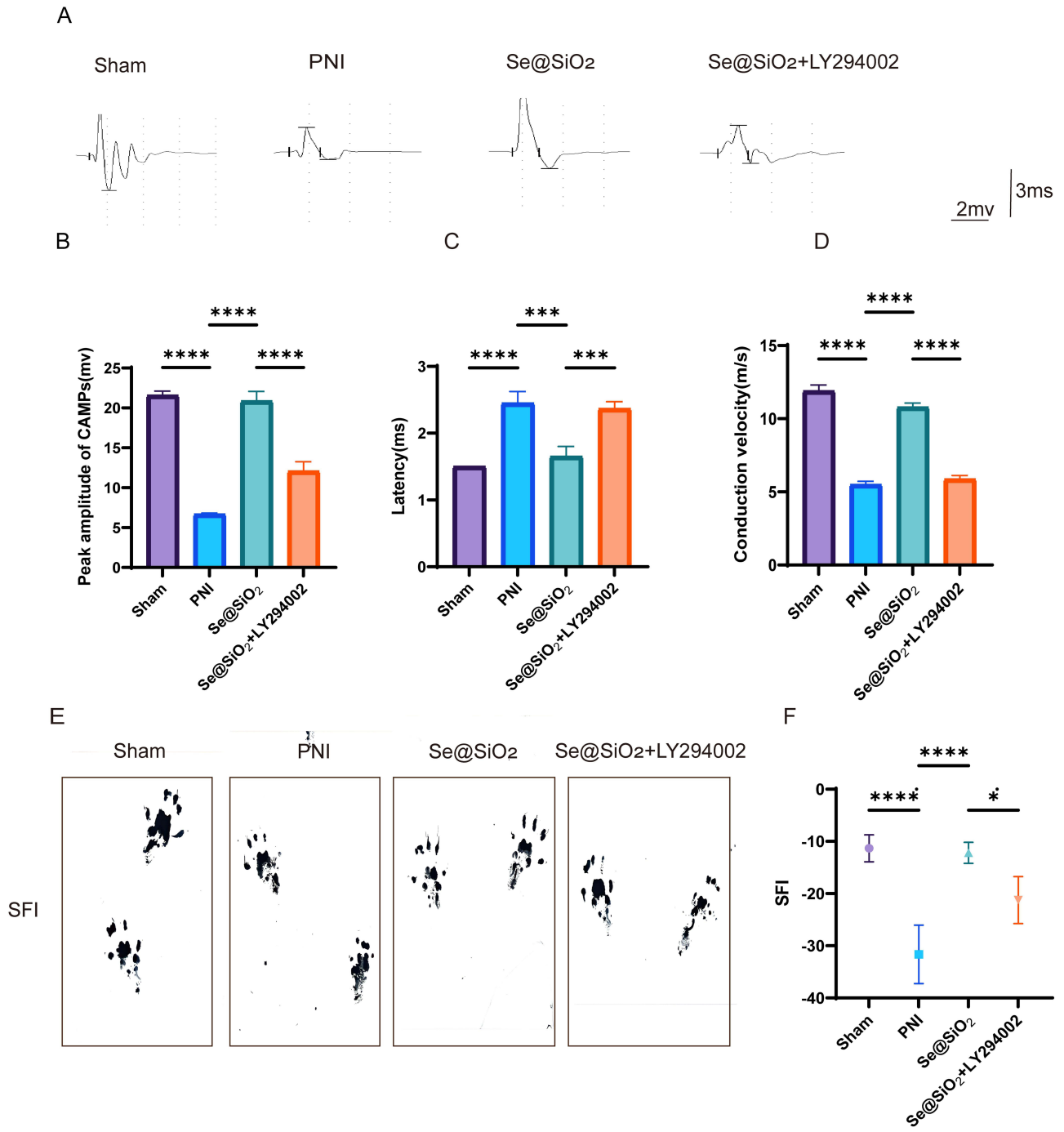

Figure 5 Se@SiO_2 NPs help to restore motor function following peripheral nerve injury (PNI). (**A**) Representative CMAPs of the injured side of rats in each group. The peak amplitude of CMAPs (**B**), conduction velocity (**C**), and latency (**D**) were statistically analyzed. (**E**) Images of footprints from rats four weeks after sciatic nerve injury. (**F**) The sciatic functional index (SFI) was statistically analyzed twenty-eight days after surgery. N = 3. *P < 0.05, ***P < 0.001 and ****P < 0.0001.

Se@SiO_2 NPs Activates the PI3K/AKT Pathway in vivo to Promote Gastrocnemius Muscle Recovery

Twenty-eight days after surgery, the gastrocnemius muscles were excised from both sides of each rat. In each group, the gastrocnemius muscles on the operated side were smaller than those on the unoperated side (Figure 6A). As illustrated in Figure 6C, the recovery rate of muscle weight was lower for the PNI and Se@SiO_2 + LY294002 groups than for the Se@SiO_2 group, and the muscle weight recovery rate for the Se@SiO_2 group was nearly identical to that for the sham

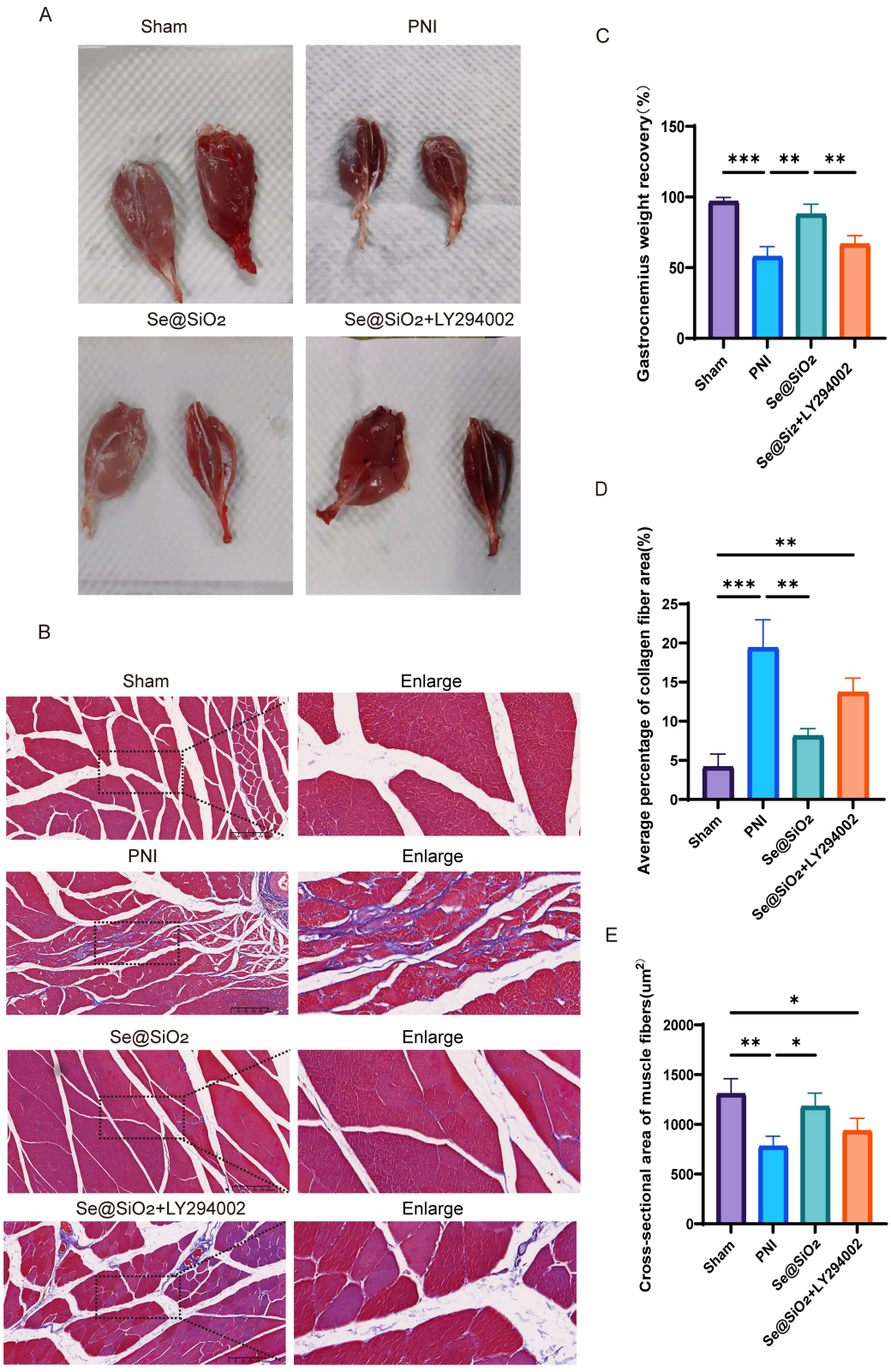

Figure 6 Se@SiO_2 NPs aid in the restoration of the gastrocnemius muscle. (**A**) Images of normal and surgically treated gastrocnemius muscles. (**B**) Images of Masson's trichrome-stained cross sections of the gastrocnemius muscle. (**C**) The gastrocnemius weight recovery ratio. (**D**) The muscle fiber cross-sectional area. (**E**) The mean proportion of the collagen fiber area. N = 3. *P < 0.05, **P < 0.01, and ***P < 0.001.

operation group. In images of Masson's trichrome-stained gastrocnemius muscles, the muscle fibers appeared red, and the collagen fibers appeared blue (Figure 6B). The cross-sectional area of the muscle fibers was notably smaller in the Se@SiO_2 group than in the PNI and Se@SiO_2 + LY294002 groups, and the cross-sectional area of the muscle fibers in the sham operation group was similar to that of the muscle fibers in the Se@SiO_2 group (Figure 6D). As depicted in Figure 6E, the percentage of the collagen fiber area in the Se@SiO_2 group was greater than that in the PNI and Se@SiO_2 + LY294002 groups but only marginally less than that in the sham operation group. These findings suggested that Se@SiO_2 NPs promotes gastrocnemius muscle recovery by activating the PI3K/AKT pathway in vivo.

Se@SiO_2 NPs Activates the PI3K/AKT Pathway in vivo to Inhibit Oxidative Stress and Suppress Inflammation Induced by Sciatic Nerve Injury

The levels of MDA, SOD, GSH, and CAT in the sciatic nerve were assessed twenty-eight days after surgery. As shown in Figure 7A, the MDA content in the PNI group prominently exceeded that in the sham operation group, but it decreased obviously after the addition of Se@SiO_2. However, an increase in the MDA content was observed after the simultaneous administration of Se@SiO_2 and LY294002, suggesting that Se@SiO_2 reduces lipid peroxidation by influencing the PI3K/AKT pathway. As depicted in Figure 7B–D, SOD activity, CAT activity, and the GSH level were markedly higher in the PNI group than in the sham operation group. Nonetheless, the administration of Se@SiO_2 notably increased SOD activity, CAT activity, and GSH levels. However, SOD activity, CAT activity, and the GSH level decreased after cotreatment with Se@SiO_2 and LY294002, indicating that Se@SiO_2 NPs can maintain the equilibrium of oxidative pressure by adjusting the PI3K/AKT pathway.

After the samples were collected, we measured the levels of anti-inflammatory factors (IL-10 and IL-4) and proinflammatory factors (IL-6 and TNF-α). We found that Se@SiO_2 significantly increased the levels of anti-inflammatory factors (IL-10 and IL-4) (Figure 7G and H) and inhibited the expression of proinflammatory factors (IL-6 and TNF-α) (Figure 7E and F), while LY294002 reversed these effects. These results suggest that Se@SiO_2 NPs can activate the PI3K/AKT pathway in vivo, which has an excellent anti-inflammatory effect.

Se@SiO_2 NPs Activates the PI3K/AKT Pathway in vivo to Inhibit Apoptosis Induced by Sciatic Nerve Injury

TUNEL staining of the sciatic nerve was assessed at twenty-eight days postsurgery (Figure 8A). As shown in Figure 8B, the proportion of apoptotic cells in the PNI group prominently exceeded that in the sham operation group, but the proportion of apoptotic cells was significantly reduced after the addition of Se@SiO_2. However, the quantity of apoptotic cells increased again after concurrent administration of Se@SiO_2 and LY294002, suggesting that Se@SiO2 NPs reduces apoptosis by affecting the PI3K/AKT pathway.

Assessment of Se@SiO_2 NPs Biosafety

In vivo studies were conducted to determine whether Se@SiO_2 causes visceral injury. No significant histological injury was detected in the hearts, livers, spleens, lungs, or kidneys of the Se@SiO_2-treated mice (Figure 9).

Discussion

In vitro and in vivo tests indicated that porous Se@SiO_2 NPs effectively promoted nerve regeneration, inhibited inflammation, significantly increased antioxidant enzyme activity, and decreased ROS levels. These effects could be ascribed to the function of oxidative stress in disrupting the balance between oxidants and antioxidants during neurological damage recovery.[38] Blocking oxidative stress following peripheral nerve damage can expedite nerve regeneration and enhance functional recovery.[39] Notably, selenium has the advantages of being economical and stable,[40] and Se is an important component of several reactive oxygen-scavenging enzymes, such as GSH-PX and thioredoxin reductase (TrxRs). TrxR plays a vital role in inhibiting oxidized H_2O_2, thioredoxin, and organic hydroperoxides.[41] Therefore, Se is crucial for safeguarding cells and tissues from oxidative damage. The Se content is directly correlated with the quantity and functionality of antioxidant proteins. By incorporating porous Se@SiO_2 NPs

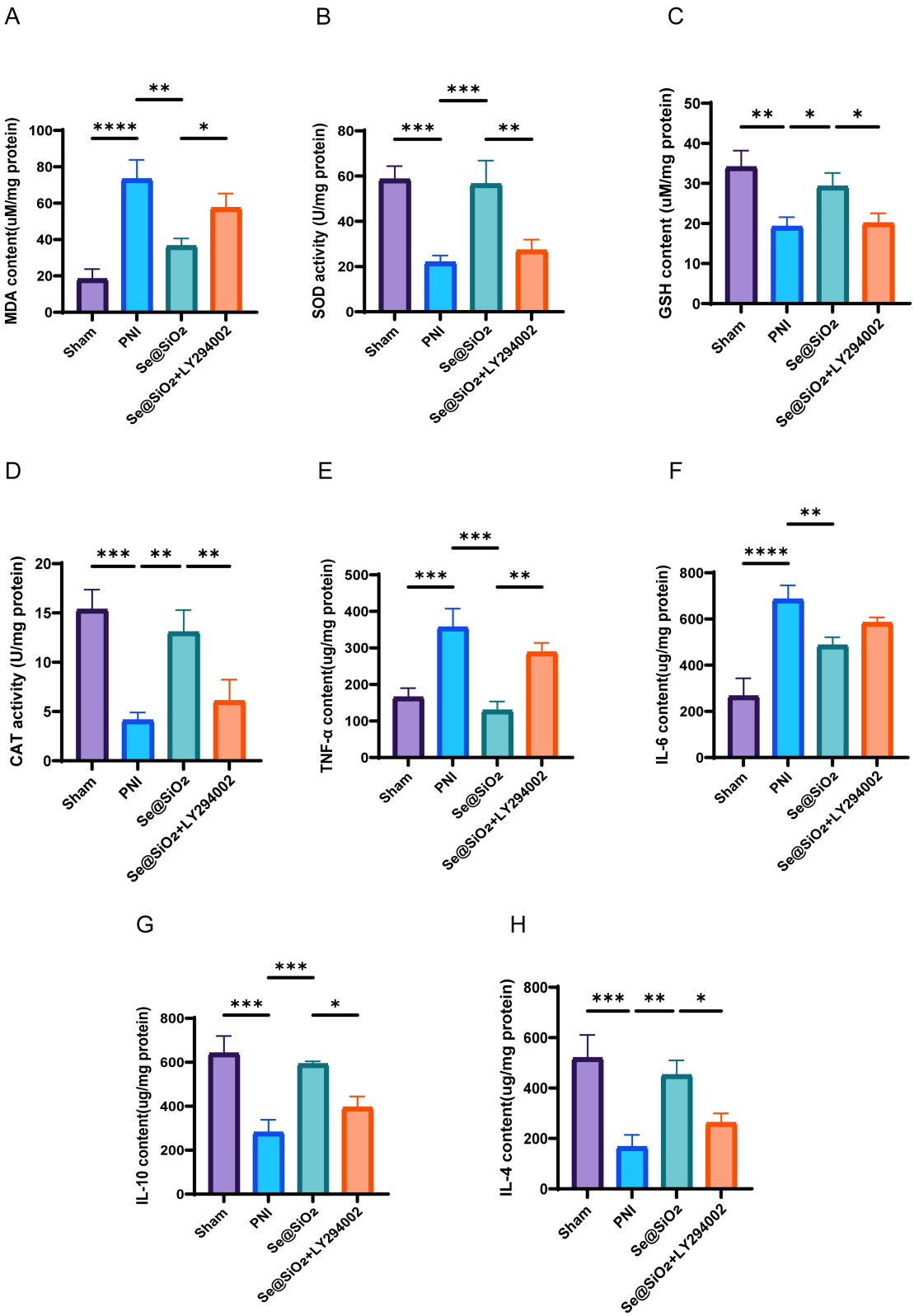

Figure 7 Se@SiO_2 effectively suppresses oxidative stress caused by PNI and is safe for use in living organisms. Twenty-eight days after sciatic nerve injury, kits were used to assess (**A**) the MDA level, (**B**) SOD activity, (**C**) GSH level, (**D**) CAT activity, (**E**) TNF-α content, (**F**) IL-6 content, (**G**) IL-10 content, and (**H**) IL-4 content. N = 3. *P < 0.05, **P < 0.01, ***P < 0.001, and ****P < 0.0001.

https://doi.org/10.2147/IJN.S460397 DovePress

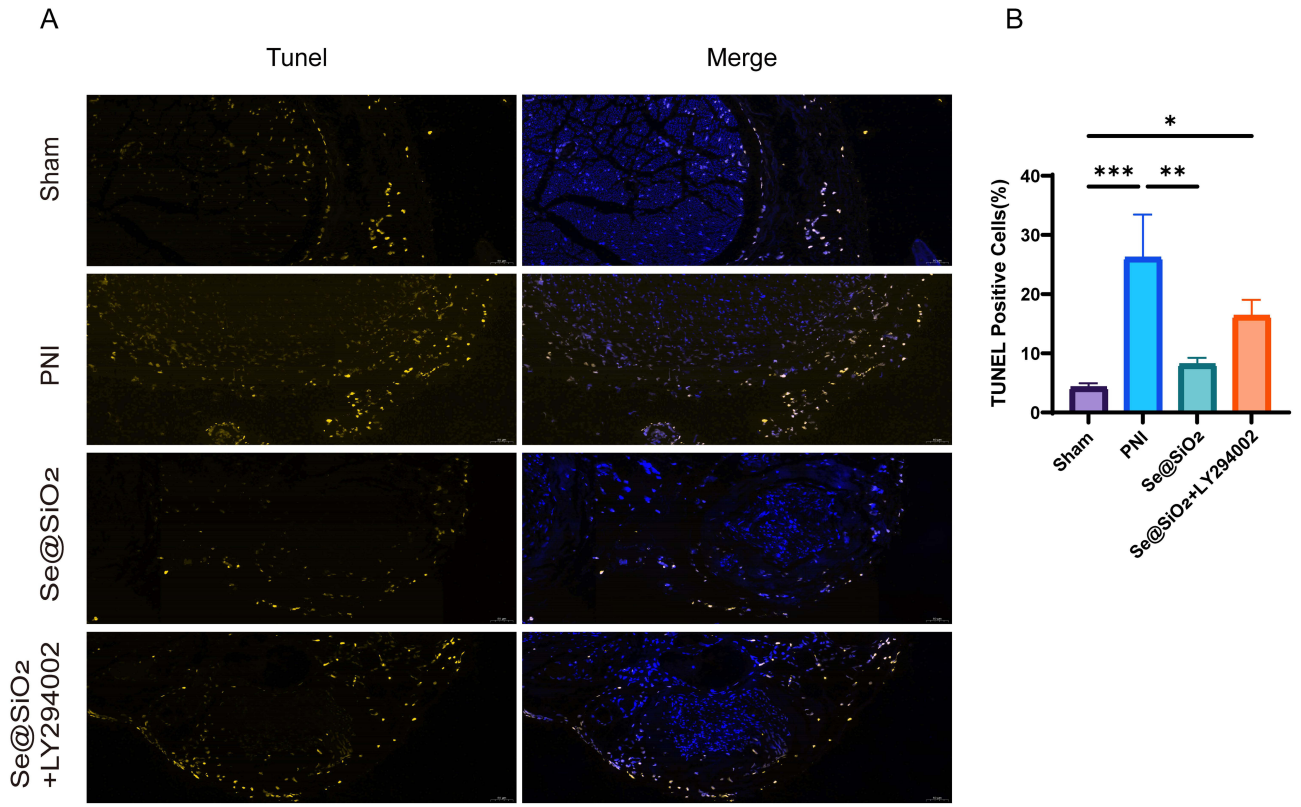

Figure 8 Se@SiO_2 effectively inhibits PNI-induced apoptosis. (**A**) Detection of apoptosis using TUNEL staining at Twenty-eight days after sciatic nerve injury. (**B**) Statistical analyses were conducted to assess the number of TUNEL-positive cells. N = 3. *P < 0.05, **P < 0.01, and ***P < 0.001.

into the system, we significantly increased the availability of the raw materials needed for antioxidant protein synthesis and enhanced the ability of these proteins to maintain an optimal oxidant–antioxidant balance within the microenvironment. Consequently, porous Se@SiO_2 NPs provide a scientifically sound option for supplementing Se and antioxidants to treat PNIs.

As shown by Western blotting, the addition of Se@SiO_2 NPs significantly upregulated Bcl-2 (an antiapoptotic protein) expression and downregulated Bax (a proapoptotic protein) expression, indicating a pronounced inhibitory impact of Se@SiO_2 NPs on apoptosis. High expression levels of the antiapoptotic protein Bcl-2 have been shown to protect neurons from apoptosis and necrosis,[42] while the proapoptotic protein Bax induces apoptosis by binding to the mitochondrial membrane, leading to an increase in the activation of proapoptotic cystathionine, which then induces cell death.[43] Moreover, the induction of apoptosis by excessive ROS after PNI is strongly linked to Bax and Bcl-2 expression levels.[44] Therefore, we hypothesize that Se attenuates SCs apoptosis by mitigating the intensity of oxidative stress and the inflammatory response related to SCs overactivation.

Myelin sheath formation is critical for axonal function.[45] In vitro experiments revealed that the expression of both PCNA and S100 increased significantly after the addition of Se@SiO_2 NPs. Both PCNA and S100 act as key marker proteins for the proliferation of SCs,[46] which suggests that Se@SiO_2 NPs can significantly promote cell proliferation and that proliferating SCs can secrete neurotrophic factors to promote neural recovery,[47] indicating that Se@SiO_2 NPs can promote axon growth and myelin regeneration by promoting SCs proliferation.

We analyzed the RNA-seq data using the KEGG database and found that Se@SiO_2 NPs were closely associated with the upregulation of the PI3K/AKT pathway. In vitro, Western blotting analysis revealed a significant increase in the p-Akt/Akt ratio in the Se@SiO_2 NPs group. Furthermore, the administration of Se@SiO_2 NPs notably decreased ROS production and apoptosis. The beneficial effects were partially reversed by inhibiting AKT phosphorylation with LY294002. The simultaneous administration of Se@SiO_2 NPs+LY294002, compared with Se@SiO_2 NPs alone, in PNI rats led to a significant decrease in

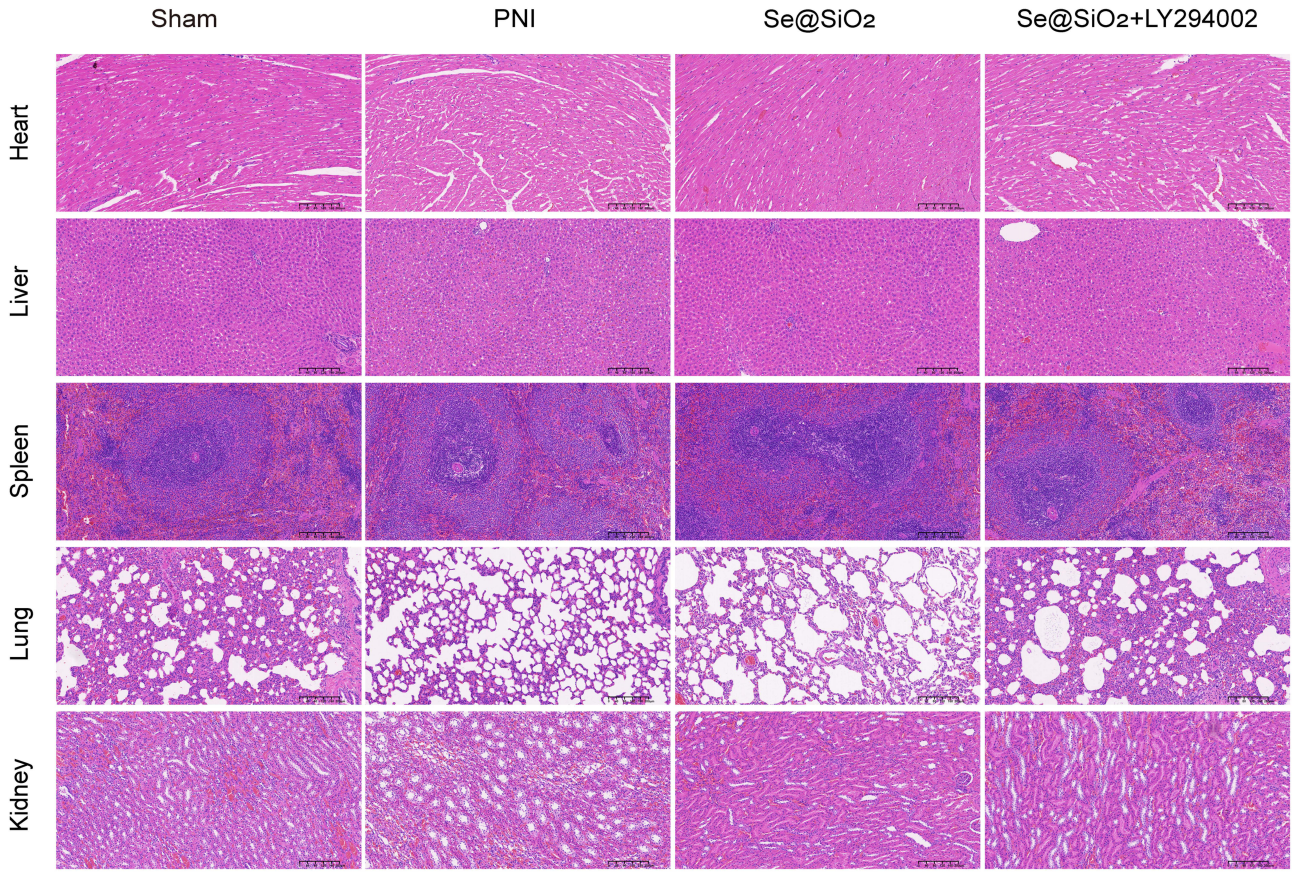

Figure 9 $Se@SiO_2$ NPs are safe for use in living organisms. Twenty-eight days after the in vivo model was established, the heart, liver, spleen, lung, and kidney tissues of the rats were subjected to histological analysis.

the myelin number, axon length, gastrocnemius muscle wet-to-weight ratio, and action potential conduction velocity. These findings suggest that the antioxidant and antiapoptotic effects of $Se@SiO_2$ NPs on nerve regeneration are partially mediated by the inhibition of the PI3K/AKT pathway. This effect is because activated AKT continues to regulate a variety of downstream target molecules, such as inhibiting proapoptotic proteins like Bax, increasing the expression of the antiapoptotic Bcl-2 protein,[48] and blocking transcription factors (eg, FOXO) from residing in the nucleus or binding to target genes.[49] This process ultimately prevents apoptosis and the transcription of genes that arrest the cell cycle. In addition, PI3K/AKT signaling has been shown to play a role in the inhibition of oxidative stress, promoting the upregulation of the expression of the Nrf2-HO-1 signaling pathway.[50] Additionally, the PI3K/AKT signaling pathway is involved in neuron differentiation, branching, and synapse formation.[51] Therefore, our study provides novel evidence supporting the promotion of nerve regeneration by $Se@SiO_2$ NPs through an antioxidant and antiapoptotic mechanism involving the activation of the PI3K/AKT pathway.

Intraperitoneal injection of $Se@SiO_2$ NPs can prevent local inflammation caused by implanted materials,[52] and $Se@SiO_2$ NPs can be absorbed and spread to other organs and damaged nerve tissues through the greater omentum into the blood circulation, which can improve the whole body and promote accelerated regeneration of peripheral nerves. HE staining of the heart, liver, spleen, lung and kidney of rats treated with $Se@SiO_2$ NPs revealed no obvious edema, congestion or tissue necrosis, indicating that $Se@SiO_2$ NPs can release Se in a controlled and slow manner and have no obvious toxic side effects but have obvious therapeutic effects. These findings further show that $Se@SiO_2$ NPs have good prospects for clinical application in peripheral nerve injury treatment.

Conclusions

The results of our research showed for the first time that the use of $Se@SiO_2$ NPs efficiently promoted SC proliferation, nerve regeneration, and functional recovery following PNI. The neuroprotective effects of $Se@SiO_2$ NP treatment might

be attributed to the inhibition of excessive oxidative stress-triggered apoptosis by activating the PI3K/AKT pathway. Se@SiO_2 NPs also have good biocompatibility, and our study could provide a very promising strategy for the clinical treatment of acute traumatic PNI using Se@SiO_2 NPs.

Data Sharing Statement

The authors declare that data supporting the findings of this study are available within the article. All relevant data can be provided by the corresponding author upon reasonable request.

Acknowledgments

This research was supported by Clinical Research Innovation Plan of Shanghai General Hospital (grant number No. CTCCR-2021B08) and the Excellent Academic Leader Project of Shanghai Science and Technology Commission (22XD1402600).

Author Contributions

All authors made a significant contribution to the work reported, whether that is in the conception, study design, execution, acquisition of data, analysis and interpretation, or in all these areas; took part in drafting, revising or critically reviewing the article; gave final approval of the version to be published; have agreed on the journal to which the article has been submitted; and agree to be accountable for all aspects of the work.

Disclosure

The authors report no conflicts of interest related to this work.

References

1. Liu F, Xu J, Liu A, et al. Development of a polyacrylamide/chitosan composite hydrogel conduit containing synergistic cues of elasticity and topographies for promoting peripheral nerve regeneration. *Biomater Sci*. 2022;10(17):4915–4932. doi:10.1039/d2bm00327a
2. Wang Q, Wang H, Ma Y, Cao X, Gao H. Effects of electroactive materials on nerve cell behaviors and applications in peripheral nerve repair. *Biomater Sci*. 2022;10(21):6061–6076. doi:10.1039/d2bm01216b
3. Okur Z, Senturk OI, Yilmaz C, et al. Promotion of neurite outgrowth by rationally designed NGF-β binding peptide nanofibers. *Biomater Sci*. 2018;6(7):1777–1790. doi:10.1039/c8bm00311d
4. Zhang S. Discovery and design of self-assembling peptides. *Interface Focus*. 2017;7(6):20170028. doi:10.1098/rsfs.2017.0028
5. Alvites R D, Branquinho M V, Sousa AC, et al. Establishment of a sheep model for hind limb peripheral nerve injury: Common peroneal nerve. *Int J Mol Sci*. 2021;22(3):1401. doi:10.3390/ijms22031401
6. Cao D, Ding J. Recent advances in regenerative biomaterials. *Regen Biomater*. 2022;9:rbac098. doi:10.1093/rb/rbac098
7. Yin Y, Li B, Yan Q, et al. Promotion of peripheral nerve regeneration and prevention of neuroma formation by PRGD/PDLLA/β-TCP conduit: report of two cases. *Regen Biomater*. 2015;2(2):119–124. doi:10.1093/rb/rbv006
8. Marqusee S, Robbins VH, Baldwin RL. Unusually stable helix formation in short alanine-based peptides. *Proc Natl Acad Sci U S A*. 1989;86(14):5286–5290. doi:10.1073/pnas.86.14.5286
9. Xue C, Kui W, Huang A, et al. Electroacupuncture suppresses neuronal ferroptosis to relieve chronic neuropathic pain. *J Cell Mol Med*. 2024;28(7):e18240. doi:10.1111/jcmm.18240
10. Norrmén C, Figlia G, Pfistner P, Pereira JA, Bachofner S, Suter U. mTORC1 Is Transiently Reactivated in Injured Nerves to Promote c-Jun Elevation and Schwann Cell Dedifferentiation. *J Neurosci*. 2018;38(20):4811–4828. doi:10.1523/JNEUROSCI.3619-17.2018
11. Chen G, Zheng Z, Sun H, et al. Dedifferentiated Schwann cells promote perineural invasion mediated by the PACAP paracrine signalling in cervical cancer. *J Cell Mol Med*. 2023;27(23):3692–3705. doi:10.1111/jcmm.17897
12. Chi M, Liu J, Li L, Zhang Y, Xie M. In-situ growth of CeO2 on biofilms: innovative nanoparticles for photothermal therapy & multi-pronged attack on Alzheimer's. *Dis Colloids Surf B Biointerfac*. 2024;238:113887. doi:10.1016/j.colsurfb.2024.113887
13. Jieensinue S, Zhu H, Li G, Dong K, Liang M, Li Y. Tanshinone IIA reduces SW837 colorectal cancer cell viability via the promotion of mitochondrial fission by activating JNK-Mff signaling pathways. *BMC Cell Biol*. 2018;19(1):21. doi:10.1186/s12860-018-0174-z
14. Dubey H, Ray A, Dubey A, Gulati K. S-Nitrosoglutathione attenuates oxidative stress and improves retention memory dysfunctions in intracerebroventricular-streptozotocin rat model of sporadic Alzheimer's disease via activation of BDNF and nuclear factor erythroid 2-related factor-2 antioxidant signaling pathway. *Neuropsychobiology*. 83:101–113. doi:10.1159/000538348
15. Ramírez-Moreno FJ, Gómez-Oliván LM, García-Medina S, Galar-Martínez M, Orozco-Hernández LA, Orozco-Hernández JM. Oxidative stress as regulator of neuronal impairment after exposure to hospital effluents in Danio rerio. *Sci Total Environ*. 2023;893:164906. doi:10.1016/j.scitotenv.2023.164906
16. Consoli V, Sorrenti V, Grosso S, Vanella L. Heme Oxygenase-1 Signaling and Redox Homeostasis in Physiopathological Conditions. *Biomolecules*. 2021;11(4):589. doi:10.3390/biom11040589
17. Yamamoto M, Kensler TW, Motohashi H. The KEAP1-NRF2 System: A thiol-based sensor-effector apparatus for maintaining redox homeostasis. *Physiol Rev*. 2018;98(3):1169–1203. doi:10.1152/physrev.00023.2017

18. Zhang Y, Liu L, Qi Y, et al. Lactic acid promotes nucleus pulposus cell senescence and corresponding intervertebral disc degeneration via interacting with Akt. *Cell Mol Life Sci*. 2024;81(1):24. doi:10.1007/s00018-023-05094-y
19. Li R, Duan W, Feng T, et al. Lycium barbarum polysaccharide inhibits ischemia-induced autophagy by promoting the biogenesis of neural stem cells-derived extracellular vesicles to enhance the delivery of miR-133a-3p. *Chin Med*. 2023;18(1):117. doi:10.1186/s13020-023-00831-8
20. Dong ZY, Pei Z, Wang YL, Li Z, Khan A, Meng XT. Ascl1 regulates electric field-induced neuronal differentiation through PI3K/Akt Pathway. *Neuroscience*. 2019;404:141–152. doi:10.1016/j.neuroscience.2019.02.004
21. Zhu W, Xue Y, Liang C, et al. S100A16 promotes cell proliferation and metastasis via AKT and ERK cell signaling pathways in human prostate cancer. *Tumour Biol*. 2016;37(9):12241–12250. doi:10.1007/s13277-016-5096-9
22. Mathews ES, Appel B. Cholesterol biosynthesis supports myelin gene expression and axon ensheathment through modulation of P13K/Akt/mTor Signaling. *J Neurosci*. 2016;36(29):7628–7639. doi:10.1523/JNEUROSCI.0726-16.2016
23. Niu S, Wang Z, Yin X, et al. A preliminary predictive model for selenium nutritional status in residents based on three selenium biomarkers. *J Trace Elem Med Biol*. 2024;81:127347. doi:10.1016/j.jtemb.2023.127347
24. Ebert R, Ulmer M, Zeck S, et al. Selenium supplementation restores the antioxidative capacity and prevents cell damage in bone marrow stromal cells in vitro. *Stem Cells*. 2006;24(5):1226–1235. doi:10.1634/stemcells.2005-0117
25. Rayman MP, Taylor EW, Zhang J. The relevance of selenium to viral disease with special reference to SARS-CoV-2 and COVID-19. *Proc Nutr Soc*. 2023;82(1):1–12. doi:10.1017/S0029665122002646
26. Legg RL, Tolman JR, Lovinger CT, Lephart ED, Setchell KD, Christensen MJ. Diets high in selenium and isoflavones decrease androgen-regulated gene expression in healthy rat dorsolateral prostate. *Reprod Biol Endocrinol*. 2008;6:57. doi:10.1186/1477-7827-6-57
27. Messarah M, Klibet F, Boumendjel A, et al. Hepatoprotective role and antioxidant capacity of selenium on arsenic-induced liver injury in rats. *Exp Toxicol Pathol*. 2012;64(3):167–174. doi:10.1016/j.etp.2010.08.002
28. Li L, Wang M, Ma YM, et al. Selenium inhibits ferroptosis in hyperglycemic cerebral ischemia/reperfusion injury by stimulating the Hippo pathway. *PLoS One*. 2023;18(9):e0291192. doi:10.1371/journal.pone.0291192
29. Fan S, Chen J, Tian H, et al. Selenium maintains intestinal epithelial cells to activate M2 macrophages against deoxynivalenol injury. *Free Radic Biol Med*. 2024;219:215–230. doi:10.1016/j.freeradbiomed.2024.04.228
30. Li H, Wang H, Cui L, et al. The effect of selenium on the proliferation of bovine endometrial epithelial cells in a lipopolysaccharide-induced damage model. *BMC Vet Res*. 2024;20(1):109. doi:10.1186/s12917-024-03958-4
31. Lai CF, Shiau FJ. Enhanced and extended ophthalmic drug delivery by pH-Triggered drug-eluting contact lenses with large-pore mesoporous silica nanoparticles. *ACS Appl Mater Inter*. 2023;15(15):18630–18638. doi:10.1021/acsami.2c22860
32. Liu X, Deng G, Wang Y, et al. A novel and facile synthesis of porous SiO2-coated ultrasmall Se particles as a drug delivery nanoplatform for efficient synergistic treatment of cancer cells. *Nanoscale*. 2016;8(16):8536–8541. doi:10.1039/c6nr02298g
33. He Y, Chen S, Liu Z, Cheng C, Li H, Wang M. Toxicity of selenium nanoparticles in male Sprague-Dawley rats at supranutritional and nonlethal levels. *Life Sci*. 2014;115(1–2):44–51. doi:10.1016/j.lfs.2014.08.023
34. Yang BY, Zhou ZY, Liu SY, et al. Porous Se@SiO2 Nanoparticles Enhance Wound Healing by ROS-PI3K/Akt Pathway in Dermal Fibroblasts and Reduce Scar Formation. *Front Bioeng Biotech*. 2022;10:852482. doi:10.3389/fbioe.2022.852482
35. Chen J, Wang Z, Zheng Z, et al. Neuron and microglia/macrophage-derived FGF10 activate neuronal FGFR2/PI3K/Akt signaling and inhibit microglia/macrophages TLR4/NF-κB-dependent neuroinflammation to improve functional recovery after spinal cord injury. *Cell Death Dis*. 2017;8(10):e3090. doi:10.1038/cddis.2017.490
36. Wu W, Liu Y, Wang Y. Sam68 promotes Schwann cell proliferation by enhancing the PI3K/Akt pathway and acts on regeneration after sciatic nerve crush. *Biochem Biophys Res Commun*. 2016;473(4):1045–1051. doi:10.1016/j.bbrc.2016.04.013
37. Sang Q, Sun D, Chen Z, Zhao W. NGF and PI3K/Akt signaling participate in the ventral motor neuronal protection of curcumin in sciatic nerve injury rat models. *Biomed Pharmacother*. 2018;103:1146–1153. doi:10.1016/j.biopha.2018.04.116
38. Wang X, Zhang G, Qiao Y, Feng C, Zhao X. Crocetin attenuates spared nerve injury-induced neuropathic pain in mice. *J Pharmacol Sci*. 2017;135(4):141–147. doi:10.1016/j.jphs.2017.08.007
39. Renno WM, Benov L, Khan KM. Possible role of antioxidative capacity of (-)-epigallocatechin-3-gallate treatment in morphological and neurobehavioral recovery after sciatic nerve crush injury. *J Neurosurg Spine*. 2017;27(5):593–613. doi:10.3171/2016.10.SPINE16218
40. Jiang H, Wang R, Zhou F, et al. Preparation, physicochemical characterization, and cytotoxicity of selenium nanoparticles stabilized by Oudemansiella raphanipies polysaccharide. *Int J Biol Macromol*. 2022;211:35–46. doi:10.1016/j.ijbiomac.2022.05.011
41. Steinbrenner H, Speckmann B, Klotz LO. Selenoproteins: antioxidant selenoenzymes and beyond. *Arch Biochem Biophys*. 2016;595:113–119. doi:10.1016/j.abb.2015.06.024
42. Tanbek K, Yuksel F, Tekin S, Tekin C, Sandal S. Asprosin improved neuronal survival by suppressing apoptosis and enhancing the activity of the autophagy pathway in the MCAO model in rats. *Eur Rev Med Pharm Sci*. 2024;28(5):1937–1946. doi:10.26355/eurrev_202403_35608
43. Chung KS, Yoo CB, Lee JH, et al. Regulation of ROS-Dependent JNK Pathway by 2'-hydroxycinnamaldehyde inducing apoptosis in human promyelocytic hl-60 leukemia cells. *Pharmaceutics*. 2021;13(11):1794. doi:10.3390/pharmaceutics13111794
44. Mahmoud MF, Rezq S, Alsemeh AE, et al. Potamogeton perfoliatus L. extract attenuates neuroinflammation and neuropathic pain in sciatic nerve chronic constriction injury-induced peripheral neuropathy in rats. *Front Pharmacol*. 2021;12:799444. doi:10.3389/fphar.2021.799444
45. Hung HA, Sun G, Keles S, Svaren J. Dynamic regulation of Schwann cell enhancers after peripheral nerve injury. *J Biol Chem*. 2015;290(11):6937–6950. doi:10.1074/jbc.M114.622878
46. Liu GM, Xu K, Li J, Luo YG. Curcumin upregulates S100 expression and improves regeneration of the sciatic nerve following its complete amputation in mice. *Neural Regen Res*. 2016;11(8):1304–1311. doi:10.4103/1673-5374.189196
47. Lindborg JA, Mack M, Zigmond RE. Neutrophils are critical for myelin removal in a peripheral nerve injury model of wallerian degeneration. *J Neurosci*. 2017;37(43):10258–10277. doi:10.1523/JNEUROSCI.2085-17.2017
48. Xu J, Ze X, Zhao L, Sheng L, Ze Y. Titanium dioxide nanoparticles oral exposure induce osteoblast apoptosis, inhibit osteogenic ability and increase lipogenesis in mouse. *Ecotoxicol Environ Saf*. 2024;277:116367. doi:10.1016/j.ecoenv.2024.116367
49. Yeh PY, Kuo SH, Yeh KH, et al. A pathway for tumor necrosis factor-alpha-induced Bcl10 nuclear translocation. Bcl10 is up-regulated by NF-kappaB and phosphorylated by Akt1 and then complexes with Bcl3 to enter the nucleus. *J Biol Chem*. 2006;281(1):167–175. doi:10.1074/jbc.M511014200

50. Chuang HY, Hsu LY, Pan CM, et al. The E3 Ubiquitin Ligase NEDD4-1 Mediates Temozolomide-Resistant Glioblastoma through PTEN Attenuation and Redox Imbalance in Nrf2-HO-1 Axis. *Int J Mol Sci*. 2021;22(19):10247. doi:10.3390/ijms221910247
51. Amaral LD, Dos Santos NA, Sisti FM, Del Bel E, Santos ACD. The antibiotic doxycycline mimics the NGF signaling in PC12 cells: A relevant mechanism for neuroprotection. *Chem Biol Interact*. 2021;341:109454. doi:10.1016/j.cbi.2021.109454
52. Pelepenko LE, Marciano MA, Francati TM, et al. Can strontium replace calcium in bioactive materials for dental applications? *J Biomed Mater Res A*. 2022;110(12):1892–1911. doi:10.1002/jbm.a.37421